Supplementary material (ESI) for Journal of Materials Chemistry

ELECTRONIC SUPPORTING INFORMATION

Efficient Acceptor Groups for NLO Chromophores: Competing Inductive and Resonance Contributions in Heterocyclic Acceptors Derived from 2-Dicyanomethylidene-3-Cyano-4,5,5-Trimethyl-2,5-Dihydrofuran

Karin Schmidt,[a] Stephen Barlow,[a] Amalia Leclercq,[a] Egbert Zojer,[b,a] Sei-Hum Jang,[c] Seth R. Marder,[a] Alex K.-Y. Jen,[c] and Jean-Luc Brédas [a]

[a] School of Chemistry and Biochemistry and
Center for Organic Photonics and Electronics
Georgia Institute of Technology
Atlanta, Georgia 30332-0400, USA

[b] Institute of Solid Physics
Graz University of Technology,
Petersgasse 16
8010 Graz, Austria

[c] Department of Materials Science and Engineering
University of Washington
Seattle, Washington 98195-2120, USA

To ensure that the trends obtained by the SOS calculations are not methodological artifacts, we have also carried out Finite Field calculations. Here, we followed the local contribution formulation[1,2] based on second derivatives of atomic charges. These were approximated by finite differences obtained from INDO[3]/HF Mulliken charges of molecules with applied electric fields between zero and $\pm 5.14 \times 10^{11}$ V/m (10^{-3} atomic units). A more detailed description of the applied methodology is given in Ref. [4].

1 P. Chopra, L. Carlacci, H. F. King, and P. N. Prasad, *J. Phys. Chem*., 1989, **93**, 7120, 1989.

2 M. N. Nakano, I. Shigemoto, S. Yamada, and K. Yamaguchi, *J. Chem. Phys.*, 1995, **103**, 4175.

3 (a) V. M. Geskin and J. L. Brédas, *J. Chem. Phys.*, 1998, **109**, 6163; (b) V. M. Geskin, C. Lambert, and J.L. Brédas, *J. Am. Chem. Soc.*, 2003, **125**, 15651; (c) D. Jacquemin, D. Beljonne, B. Champagne, V. M. Geskin, J. L. Bredas, J. M. Andre, *J. Chem. Phys.*, 2001, **115**, 6766.

4 A. Leclercq, E. Zojer, S.-H. Jang, S. Barlow, V. Geskin, A. K.-Y. Jen, S.R. Marder, and J.L. Brédas, *J. Chem. Phys.*, 2006, 1**24**, 044510.

TABLES

Table S1: Orientationally averaged second-order polarizabilities ($\langle\beta\rangle = \{\beta_x^2 + \beta_y^2 + \beta_z^2\}^{1/2}$), long-axis components of the second-order polarizability (β_{xxx}) for both SOS and FF values, and the second-order molecular polarizabilities (β_{xxx}) calculated with the two-state model for chromophores **1** to **10**.

chromophore	X	$\langle\beta\rangle$ (10^{-30} esu) SCI /SOS	β_{xxx} (10^{-30} esu) SCI/SOS	β_{xxx} (10^{-30} esu) FF	β_{xxx} (10^{-30} esu) two-state model
1	SiH_2	310	301	336	502
2	CH_2	315	314	355	520
3	$C=CH_2$	352	350	387	578
4	NH	281	290	330	471
5	CO	467	443	487	755
6	S	323	321	362	532
7	O	316	320	368	499
8	$C=CHNO_2$	506	489	543	833
9	SO	393	379	430	639
10	SO_2	500	476	536	761

Table S2: Transition energies (E_{ge}), x-component of the dipole moments for the ground state ($\mu_{g,x}$) and the dominant electronic excited state ($\mu_{e,x}$), the change in state dipole moments ($\Delta\mu_{ge,x}$), and the transition dipole moment ($\mu_{ge,x}$) values calculated with INDO/SCI/SOS method for chromophores **1** to **10**.

chromophore	E_{ge} *(eV)*	$\mu_{g,x}$ *(D)*	$\mu_{e,x}$ *(D)*	$\Delta\mu_{ge,x}$ *(D)*	$\mu_{ge,x}$ *(D)*
1	2.50	6.1	15.4	9.3	12.0
2	2.49	7.7	16.8	9.1	12.3
3	2.48	7.0	17.2	10.2	12.2
4	2.52	8.6	17.2	8.6	12.2
5	2.37	11.2	23.1	11.9	12.4
6	2.49	9.8	19.3	9.5	12.2
7	2.48	11.1	19.8	8.7	12.1
8	2.34	10.7	23.9	13.3	12.1
9	2.43	13.5	24.3	10.8	12.2
10	2.33	15.5	27.1	11.6	12.3

Table S3: Orientationally averaged second-order polarizabilities ($<\beta> = \{\beta_x^2 + \beta_y^2 + \beta_z^2\}^{1/2}$), long-axis components of the second-order polarizability (β_{xxx}) for both SOS and FF values, and the second-order molecular polarizabilities (β_{xxx}) calculated with the two-state model for chromophores **11** to **20**.

chromophore	X	$<\beta>$ (10^{-30} esu) SCI /SOS	β_{xxx} (10^{-30} esu) SCI/SOS	β_{xxx} (10^{-30} esu) FF	β_{xxx} (10^{-30} esu) two-state model
11	SiH_2	134	145	140	271
12	CH_2	130	140	140	257
13	$C=CH_2$	156	170	160	307
14	NH	107	116	117	183
15	CO	210	225	203	427
16	S	134	144	140	267
17	O	122	131	133	233
18	$C=CHNO_2$	191	205	187	339
19	SO	163	176	167	335
20	SO_2	212	226	209	404

Table S4: Transition energies (E_{ge}), x-component of the dipole moments for the ground state ($\mu_{g,x}$) and the dominant electronic excited state ($\mu_{e,x}$), the change in state dipole moments ($\Delta\mu_{ge,x}$), and the transition dipole moment ($\mu_{ge,x}$) values calculated with INDO/SCI/SOS method for chromophores **11** to **20**.

chromophore	E_{ge} *(eV)*	$\mu_{g,x}$ *(D)*	$\mu_{e,x}$ *(D)*	$\Delta\mu_{ge,x}$ *(D)*	$\mu_{ge,x}$ *(D)*
11	3.04	9.4	17.7	8.3	11.4
12	3.03	10.6	18.0	7.4	11.7
13	2.98	10.2	19.2	9.1	11.4
14	3.08	11.8	17.4	5.7	11.5
15	2.83	12.5	23.9	11.4	11.3
16	3.03	12.2	20.2	8.0	11.5
17	3.04	11.0	17.2	6.2	12.0
18	2.84	14.7	26.3	11.6	9.6
19	2.96	14.3	24.1	9.8	11.3
20	2.85	15.8	26.4	10.6	11.5

Figure S1: Calculated values for β_{xxx} (a) derived from the two-state expression, considering only the first intense excited state, with the corresponding change in state dipole moment ($\Delta\mu_{ge,x}$, open squares) and the reciprocal of the square of the transition energy ($1/E_{ge}^2$, solid squares) shown in (b), for chromophores **11** to **20**.

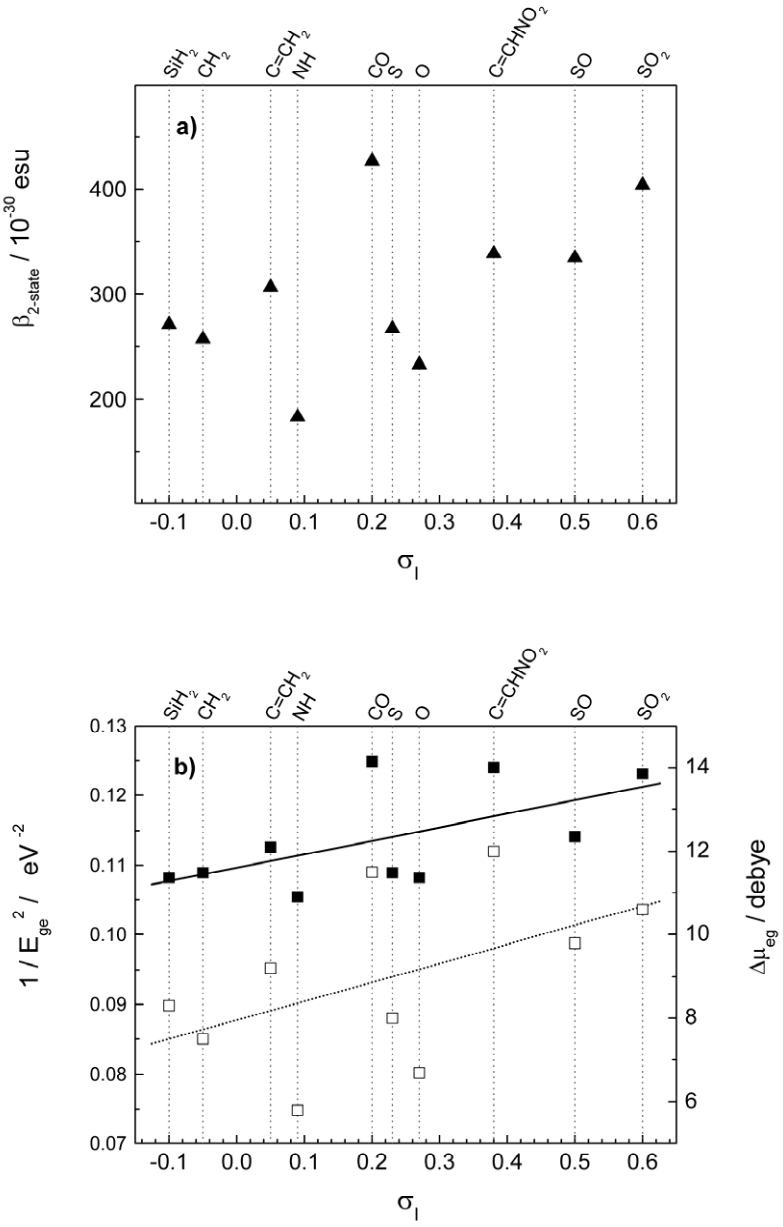

Table S5: Orientationally averaged second-order polarizabilities ($<\beta> = \{\beta_x^2 + \beta_y^2 + \beta_z^2\}^{1/2}$), long-axis components of the second-order polarizability (β_{xxx}) for both SOS and FF values, and the second-order molecular polarizabilities (β_{xxx}) calculated with the two-state model for chromophores **21** to **30**.

chromophore	X	$<\beta>$ (10^{-30} esu) SCI /SOS	β_{xxx} (10^{-30} esu) SCI/SOS	β_{xxx} (10^{-30} esu) FF	β_{xxx} (10^{-30} esu) two-state model
21	SiH_2	278	293	263	605
22	CH_2	277	290	263	520
23	$C=CH_2$	279	288	264	487
24	NH	265	275	255	525
25	CO	364	375	327	443
26	S	308	323	286	558
27	O	296	307	277	569
28	$C=CHNO_2$	326	334	301	423
29	SO	370	389	339	162
30	SO_2	454	476	405	650

Table S6: Transition energies (E_{ge}), x-component of the dipole moments for the ground state ($\mu_{g,x}$) and the dominant electronic excited state ($\mu_{e,x}$), the change in state dipole moments ($\Delta\mu_{ge,x}$), and the transition dipole moment ($\mu_{ge,x}$) values calculated with method for chromophores **21** to **30**. In addition, the corresponding INDO/SCI/SOS calculated parameters $E_{ge'}$, $\mu_{e',x}$, $\Delta\mu_{ge',x}$, and the transition dipole moments $\mu_{ge',x}$ and $\mu_{ee',x}$ (with their sign relative to $\mu_{ge,x}$) for the excited state e' are given for chromophores **25** and **28** to **30**.

chromophore	E_{ge} *(eV)*	$\mu_{g,x}$ *(D)*	$\mu_{e,x}$ *(D)*	$\Delta\mu_{ge,x}$ *(D)*	$\mu_{ge,x}$ *(D)*	$E_{ge'}$ *(eV)*	$\mu_{ee',x}$ *(D)*	$\mu_{e',x}$ *(D)*	$\Delta\mu_{ge',x}$ *(D)*	$\mu_{ge',x}$ *(D)*
21	2.63	6.6	18.9	12.3	10.9					
22	2.66	8.2	20.4	12.2	11.4					
23	2.67	7.5	19.8	12.3	11.0					
24	2.62	8.7	21.5	12.8	11.0					
25	2.57	10.5	22.0	11.5	10.4	2.85	-2.9	22.7	12.2	-5.6
26	2.57	9.4	22.5	13.1	11.0					
27	2.63	11.0	23.5	12.5	11.6					
28	2.61	12.2	24.0	11.7	10.2	2.89	1.4	25.9	13.7	-3.6
29	2.44	11.5	17.6	6.1	8.2	2.51	-7.9	16.3	4.9	-7.1
30	2.33	13.1	26.5	13.5	10.6	3.43	-8.0	15.4	2.3	-3.6

Figure S3: Evolution of β_{xxx} as a function of intermediate states normalized to the converged β_{xxx} value for chromophores **1** to **30**.[a)]

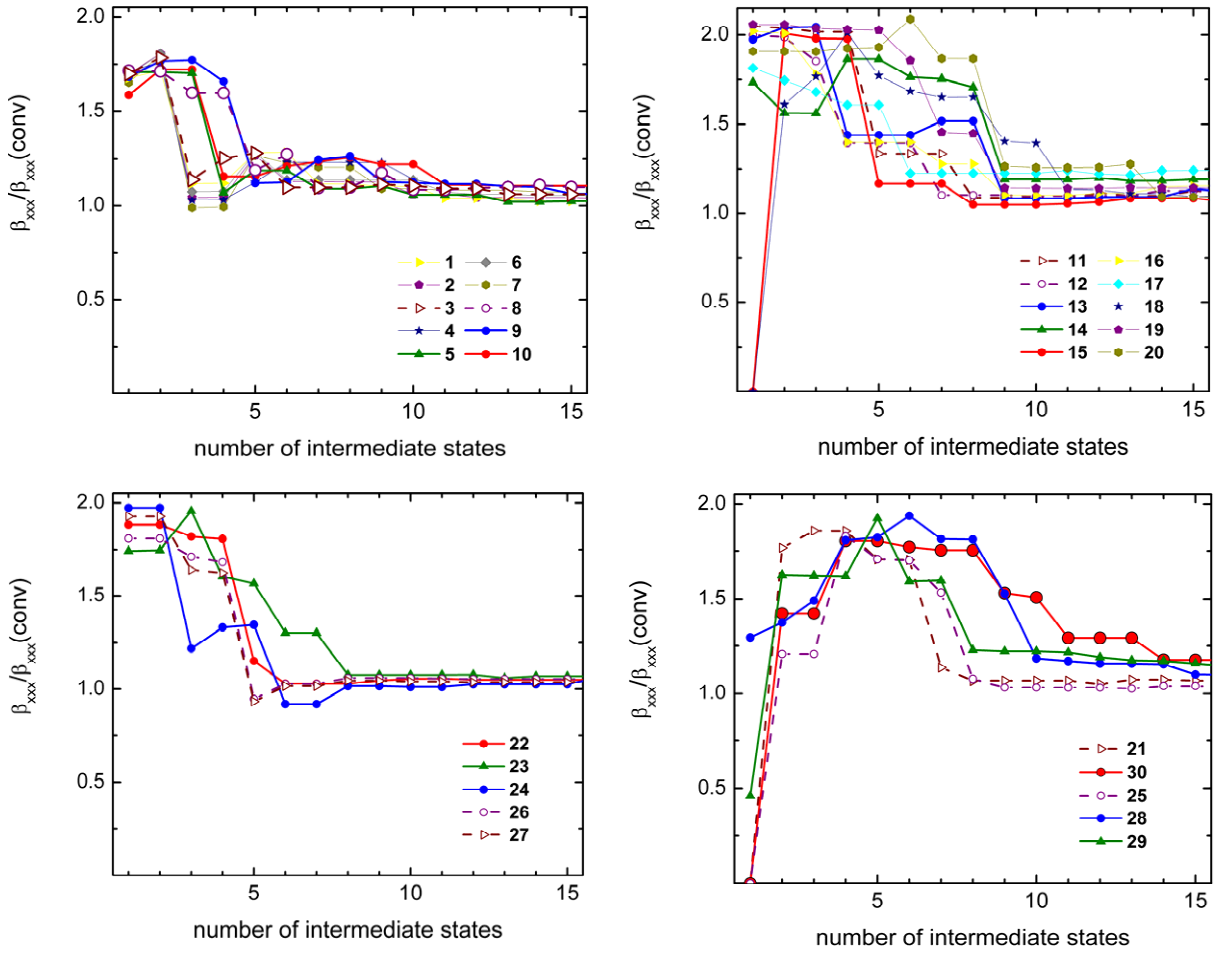

a) The convergence plots for **21**, **25**, and **28** - **30** (lower right panel) have been separated from the rest of the series **22** - **24**, **26**, **27** (lower left panel) to illustrate their distinctively different convergence behavior.

We note that the convergence pattern is similar in **1**-**10** (upper left panel); the first excited state *e* gives rise to the largest contribution to β which is partially compensated by a higher-lying state *e'*. The ratio between the *e*- and the *e'*-related β contributions essentially remains constant in **1**-**10**. In **11**-**20** (upper right panel), again the first (or the second in **15** and **18**) excited state *e* gives rise to the largest contribution to $\beta_{initial}$. This initial $\beta_{initial}$ value is partially compensated by either one or multiple higher-lying excited states; however, the combined contribution of the latter relative to $\beta_{initial}$ is constant. However, not all compounds in **21**-**30** (lower panels) share a convergence behavior similar to the one observed in **1**-**20**. While in **21**-**24**, **26** and **27** the initial $\beta_{initial}$ value is essentially built up by one excited state *e*, at least two low-lying excited states with large μ_{ge} contribute to $\beta_{initial}$ in **25** and **28**-**30** (see also Figure S4). As a consequence, a two-state model cannot

account for the evolution of the converged β in **21**-**30**, since it would not consider one of these two strongly participating states in **25** and **28**-**30**.

Figure S4: Evolution of β_{xxx} (normalized to the converged β_{xxx}) as a function of intermediate states for chromophore **25**.

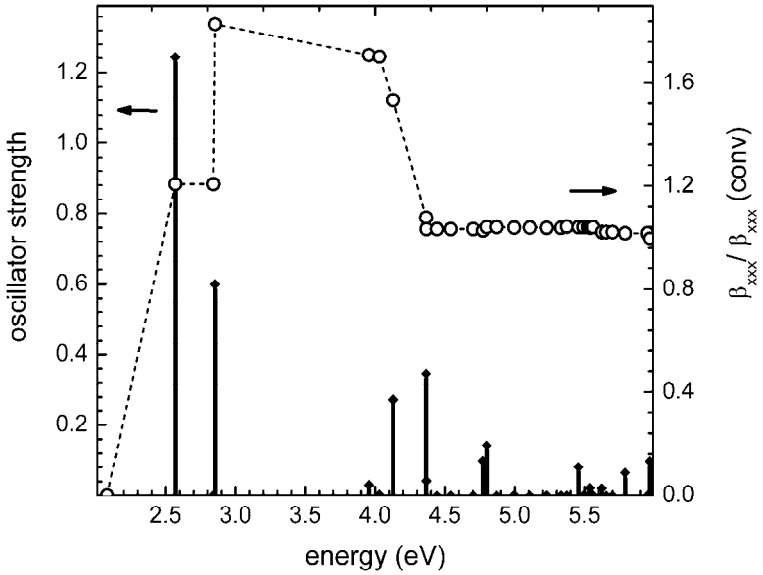

Figure S5: Calculated values for β_{xxx} derived from the two-state (solid squares) and three-state (open-square) expression, considering only the lowest (two) excited state(s) with significantly large oscillator strength for chromophores **21** to **30**.